Draft version December 9, 2024
Typeset using LaTeX **twocolumn** style in AASTeX63

ABYSS III: Observing accretion activity in young stars through empirical veiling measurements

Serat Saad,[1] Marina Kounkel,[2] Keivan G. Stassun,[1] A. Roman-Lopes,[3] C. Román-Zúñiga,[4] Jinyoung Serena Kim,[5] and etc

[1] *Department of Physics and Astronomy, Vanderbilt University, VU Station 1807, Nashville, TN 37235, USA*
[2] *Department of Physics and Astronomy, University of North Florida, 1 UNF Dr, Jacksonville, FL, 32224, USA*
[3] *Department of Astronomy, Universidad de La Serena, Av. Raul Bitran #1302, La Serena, 170000, Chile*
[4] *Universidad Nacional Autónoma de México, Instituto de Astronomía, AP 106, Ensenada 22800, BC, México*
[5] *Steward Observatory, University of Arizona, 933 N. Cherry Ave., Tucson, AZ 85721-0065, USA*

ABSTRACT

Stellar accretion plays an important role in the early stages of stellar evolution, particularly in Classical T Tauri Stars (CTTSs). Accretion of a CTTS can be related to different physical parameters like effective temperature ($T_{\rm eff}$), age, abundace of hydrogen, etc. We can infer how accretion works by examining it across different wavelength regions. Accretion can be traced using veiling, a parameter that measures how excess emission from accretion affects the CTTSs's photospheric spectrum. In this study, we selected a sample of CTTSs, Weak-line T Tauri Stars (WTTSs), and field stars, observed with the BOSS spectrograph from SDSS-V. First, measured veiling for CTTSs through comparing them to theoretical spectra. Next, we compared the veiling of CTTSs to their physical properties, including wavelength, Hα emission, effective temperature, and age. We investigated how veiling is changing with these parameters and what can be the physical reasons behind the changes. Finally, we evaluated how our findings align with existing accretion shock models. This study highlights veiling as a critical diagnostic tool for understanding accretion in young stars.

Keywords: accretion, accretion disks - stars, veiling

1. INTRODUCTION

Accretion process plays a crucial role in the early stages of stellar evolution, particularly in a type of young stars known as Classical T Tauri Stars (CTTSs). These stars are magnetically active and accrete material from their surrounding circumstellar disks, which are the birthplaces of future exoplanets (Hartmann et al. 2016). The period of planet formation coincides with that of star formation, and accretion processes significantly influence the lifespan of these disks, typically lasting a few million years (Hartmann et al. 2016). Accretion not only affects the mass transfer to the star but also plays a crucial role in angular momentum evolution and jet launching (Fischer et al. 2023). Therefore, understanding accretion is vital for developing comprehensive theories of stellar and planetary formation.

In the magnetospheric accretion model (Shu et al. 1994; Romanova et al. 2002; Bessolaz et al. 2008; Hartmann et al. 2016), the magnetic field of a CTTS truncates the inner disk at a few stellar radii, channeling the disk material into accretion columns that fall onto the star at nearly free-fall velocities. This process generates accretion shocks, leading to emission lines and excess continuum emission superimposed on the star's photospheric spectrum, a phenomenon known as veiling (Calvet & Gullbring 1998). Veiling (r_λ) can be defined as following:

$$F_{\rm source,\,\lambda} = \frac{F_{\rm phot,\,\lambda} + r_\lambda}{(1 + r_\lambda)} \tag{1}$$

where, $F_{\rm source,\,\lambda}$ is the total flux coming from the source, $F_{\rm phot,\,\lambda}$ is the photospheric, and r_λ is the veiling.

High veiling values indicate substantial ongoing accretion, which can significantly influence the thermal and chemical properties of the disk and affect the conditions under which planets form (Morbidelli & Raymond 2016).

The mass accretion rate ($\dot{M}_{\rm acc}$) is a critical parameter in studying the evolution of pre-main sequence stars and their disks. It can be estimated from the accretion luminosity ($L_{\rm acc}$), which is derived from accretion-powered emission lines using empirical relations (Gullbring et al.

marina.kounkel@unf.edu

1998; Alcalá et al. 2017). Alternatively, $\dot{M}_{\rm acc}$ can be inferred by comparing veiling values to accretion shock models. These models, initially one-dimensional and plane-parallel (Calvet & Gullbring 1998), have evolved to incorporate multiple energy fluxes and filling factors, allowing for complex accretion column structures (Ingleby et al. 2013; Robinson & Espaillat 2019; Espaillat et al. 2022; Pittman et al. 2022). Optical veiling can also be used to infer accretion luminosity, as demonstrated by studies like Stock et al. (2022). Analyzing the relationship between veiling and stellar rotation provides further insights into the dynamics of accretion processes.

Traditionally, veiling has been assumed to be constant across different wavelengths, typically modeled using a handful of discrete lines (Bertout 1989; Gahm et al. 2008). Only a few of the studies have been done where veiling has been compared with wavelength (Basri & Batalha 1990; Ingleby et al. 2013). Theoretical models suggest that veiling should vary as a function of wavelength due to the different physical conditions in the accretion stream and the circumstellar environment(Calvet & Gullbring 1998).

Empirical profiles of veiling across a broad range of wavelengths are sparse, limiting our understanding of accretion processes in young stars. So, assuming veiling to be constant across different wavelengths may not capture the true complexity of the accretion processes. Understanding how veiling varies with wavelength can provide insights into the structure and dynamics of the accretion flows in CTTSs.

The Sloan Digital Sky Survey in its fifth iteration (SDSS-V), has obtained an unprecedented sample of optical and near IR spectra of millions of stars using the BOSS (Baryonic Oscillation Spectroscopic Survey) and APOGEE (Apache Point Observatory Galactic Evolution Experiment) spectrographs. The SDSS-V Milky Way Mapper (MWM) program, through the APOGEE & BOSS Young Star Survey (ABYSS), aims to achieve high-resolution, multi-epoch spectra of over 100,000 young stars with ages less than 30 Myr. This will provide a unique opportunity for statistical analysis of accretion processes (Kounkel et al. 2023). In the ABYSS program, more than 18,000 young stars, including over 5,500 CTTSs, have been identified using a newly developed method (Saad et al. 2024).

In this paper, we aim to use SDSS optical spectra to examine the veiling in CTTSs, its dependence on wavelength, and its variation with different physical properties such as effective temperature, age, and the equivalent width of the Hα line. In Section 2, we describe the data used for our analysis, including the sources of the spectra and the methods for extracting stellar parameters. In Section 3, we detail the analysis methods, including the correction for extinction and the calculation of veiling across different wavelength bins. We also discuss the empirical methods used to measure veiling without assuming a specific model. In Section 4, we present the results of our veiling measurements, comparing veiling values across different temperature and age bins, and examining their consistency. Finally, in Section 5, we discuss the implications of our findings for understanding accretion processes in CTTSs and compare our results with theoretical models and previous empirical studies. We conclude in Section 6 with a summary of our findings and their significance for future research on accretion in young stellar objects.

2. DATA

BOSS is a low-resolution spectrograph operated by the SDSS-V. There are two 2.5-meter telescopes: one located in the northern hemisphere at the Apache Point Observatory (APO) and the other in the southern hemisphere at the Las Campanas Observatory (LCO). The strategic positioning of these observatories allows for comprehensive sky coverage, capturing spectra from both hemispheres. BOSS covers a wavelength range of 3600-10400 Å, with a resolving power of R$\sim$1800 and a pixel scale of $\sim$1 Å(Smee et al. 2013). Each spectrograph at APO and LCO is capable of observing 500 spectra simultaneously within a field of view of 3° and 2°, respectively. The APOGEE and BOSS Young Star Survey (ABYSS) program within SDSS-V focuses on obtaining spectra of approximately 100,000 young stars (Kounkel et al. 2023). Since its initiation in 2021, BOSS has observed over a million stars, among which 40,000 of these targets being young stars identified by the ABYSS program.

We extracted fundamental stellar parameters of the sources observed by BOSS using BOSS Net, an advanced neural network. These parameters include effective temperature ($T_{\rm eff}$), surface gravity ($\log g$), metallicity ([Fe/H]), and radial velocity (RV) (Sizemore et al. 2024). The BOSS Net can predict $T_{\rm eff}$ with a precision of 0.008 dex and $\log g$ with a precision of 0.1 dex at a signal-to-noise ratio (SNR) of approximately 15, calibrated to theoretical models and specifically calibrated for YSOs. Accurate RVs are essential for precisely identifying spectral lines, especially those that are weak and narrow.

In (Saad et al. 2024) we developed a pipeline to measure the equivalent widths and identifying the young stars based on them. Spectral lines, such as Li I, optical H I, and Ca II, are excellent indicators of stellar youth and can be used to distinguish young stars from

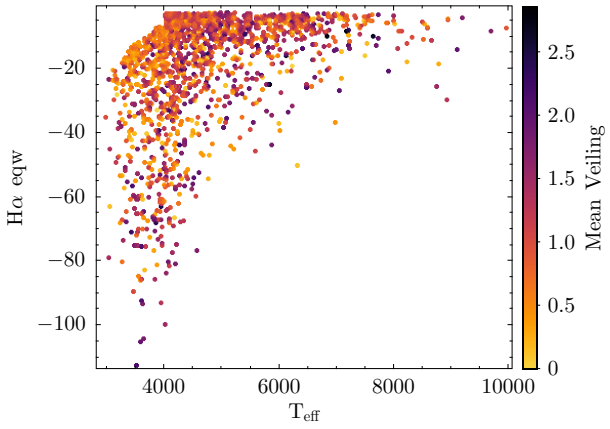

Figure 1. Plotted Hα eqw vs $T_{\rm eff}$ of our sample color coded by mean veiling for each of the sources.

other sources. These lines either appear in emission or absorption, depending on the physical conditions of the star and its surrounding environment. For example, the presence of the Li I 6708 Å absorption line is a direct indicator of stellar youth, as lithium is rapidly depleted in stars older than a few million years. Similarly, optical H I lines, such as Hα, often appear in strong emission in young stars due to accretion processes, and Ca II lines are associated with chromospheric activity, which is more prominent in younger stars. LINEFOREST can estimate the equivalent widths of 50 different youth-sensitive line regions of any optical spectra of a star. The pipeline then applies a set of criteria based on the properties of the spectral lines to identify young stars that have age < 30 Myr. In (Saad et al. 2024), we also developed a technique that can predict whether any of these young stars are classical T Tauri stars (CTTSs) or not. This developed technique is based on the equivalent width of the Hα line, a good indicator of strong accretion activity. Based on this pipeline and method we identified around 40,000 young stars and around 1900 CTTSs. Figure 1 shows us the distribution of the $T_{\rm eff}$ and Hα eqw of the sources. We used these sources in this work to do further analysis to understand their accretion process.

We inferred the ages for each of these selected sources using Sagitta (McBride et al. 2021). Sagitta is a neural net that first identifies stars that are in pre-main sequence and then calculate their ages based on photomoetry, parallax, and average extinction. Comparing to the traditional techniques that relies on theoretical isochrones for predicting ages, Sagitta offers more stable performance with respect to $T_{\rm eff}$ (Kounkel et al. 2023).

3. ANALYSIS

To measure extinction and veiling in the spectra it is necessary to compare the spectrum of CTTS with another stellar spectra that is not affected by either extinction or the accretion stream. To address this, we used synthetic PHOENIX spectra, which are high-resolution spectral templates created for a wide range of stellar parameters across various wavelength ranges (optical, near-infrared, infrared, and ultraviolet) (Husser et al. 2013). The PHOENIX library covers a parameter space of: effective temperature ($T_{\rm eff}$) from 2300 K to 12,000 K, surface gravity ($\log g$) from 0.0 to +6.0, metallicity ([Fe/H]) from -4.0 to +1.0, and alpha enhancement ([α/Fe]) from -0.2 to +1.2. We used [Fe/H] = 0 and [α/Fe] = 0 for our models to ensure a consistent baseline, as these values represent solar metallicity and no alpha enhancement, which are typical for the young stars we are studying (Kounkel et al. 2023; Saad et al. 2024). Using these templates, we can perform spectral corrections and analyses on the observed CTTSs spectra.

3.1. *De-reddening Spectra*

The first step was to correct for extinction (reddening) in the spectra. Extinction is not the only one, but a dominant source of discrepancy between the synthetic model and the observed spectra other than the accretion. Though extinction can be stronger in blue and weaker in red, it can be characterized using a single coefficient (A_V). The observed spectra were first matched with the corresponding synthetic spectra from the PHOENIX library. We first performed a sub grid interpolation between the observed spectra and the synthetic spectra to match physical parameters like $T_{\rm eff}$ and $\log g$. Then we compared each observed spectrum to the corresponding synthetic spectrum using G23 model of python 'dust_extinction' library (Gordon 2024). This helped us to calculate the extinction parameter (A_V) for each spectrum. Once the $A_V$was determined, we de-reddened the spectra through dividing by the extinction profile. This de-reddened spectra was then further used for calculating veiling.

Figure 2 shows the on sky distribution of identified young star candidates, with colors indicating the extinction parameter (A_V). Higher extinction is concentrated along the Galactic plane where dust density is greater. Figure 3 displays the spatial distribution of young star candidates in Cartesian coordinates also color coded by (A_V). The radial pattern shows how extinction varies with distance. It reflects the structure of dust clouds along different sight lines.

3.2. *Measuring Veiling*

The next step is to measure the veiling profile for all the sources. Veiling (r_λ) can be defined using Equa-

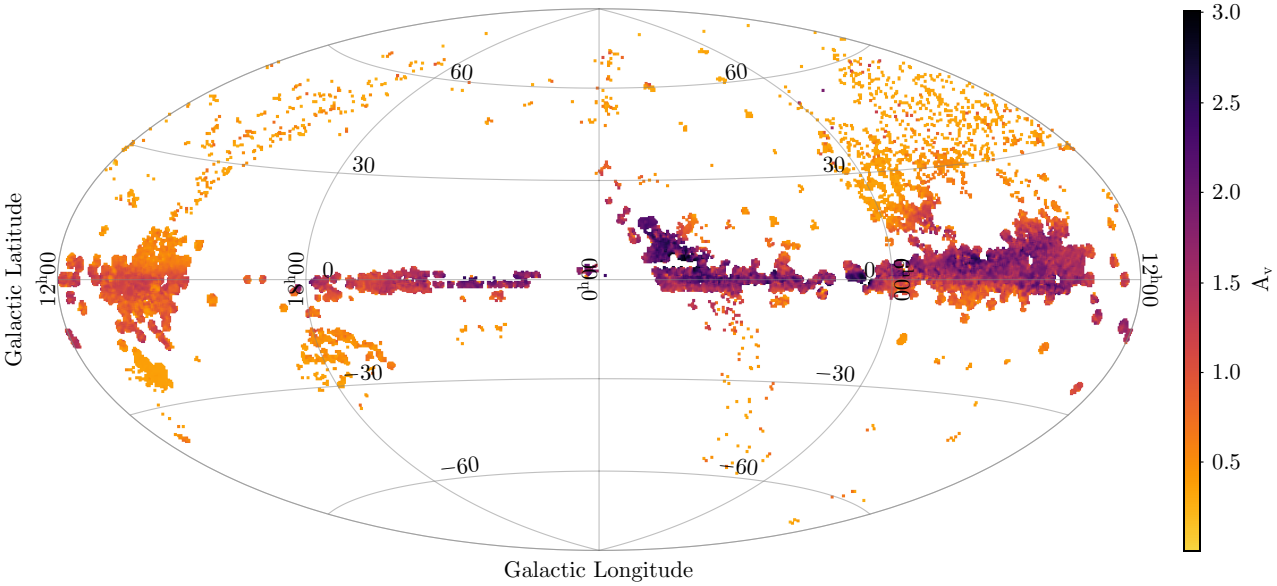

Figure 2. On-sky distribution of identified YSO candidates with the calculated extinction parameter (A_v).

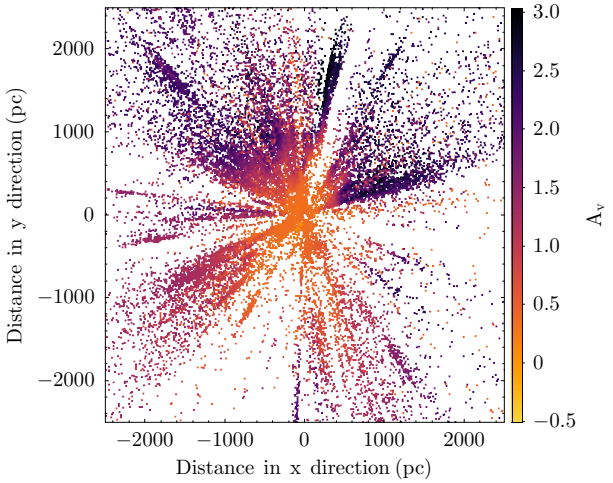

Figure 3. Distribution of the sources in space color coded by the extinction parameter (A_v).

tion 1. Veiling depends on wavelengths and, unlike A_V, it cannot be characterized with a single constant. So, we empirically calculated veiling at various wavelength ranges without assuming any model for it. At first we interpolated the extinction corrected spectra with the corresponding synthetic spectra for each of the sources for common wavelength grid. Then we divided both the synthetic spectra and the observed spectra in different wavelength bins. The chosen wavelength bins were 1000 Å wide with advancing in steps of 100 Å, for the total BOSS spectra wavelength range of 3600-10000 Å. Using individual lines to calculate veiling can limit us to isolated regions of the spectrum with missing subtle variations and wavelength dependent trends in veiling that could provide insights into the broader accretion structure. So instead of using individual lines to measure veiling, we chose an empirical approach across broader wavelength bins.

To calculate the veiling for each wavelength bins, we performed a least square optimization between the observed spectra and the corresponding PHOENIX template. In that case, each of the wavelength bins were allowed to have the best r_λ for equation 1, where $F_{\mathrm{phot},\,\lambda}$ is the synthetic flux coming from the PHOENIX template. Figure 4 illustrates the observed spectra (blue), extinction-corrected spectra (purple), and veiling + extinction-corrected spectra (green) compared to the synthetic PHOENIX spectra (red). The veiling + extinction-corrected spectra represent the star's photosphere, with veiling increasing and extinction decreasing the flux. All spectra are normalized for clarity.

We performed our analysis and veiling measurements for all the sources, including all of Classical T-Tauri Stars (CTTSs), Weak-lined T-Tauri Stars (WTTSs), and some field stars. Analysis for WTTSs and field stars may seem unnecessary because of the lack of accretion disk, but we performed the analysis for these sources to understand the systematic biases behind our approach.

In doing this we have obtained independent measurement of veiling (r_λ) for a total of ∼70 unique measurements per spectrum at different mean wavelengths for all the CTTSs, WTTSs, and selected field stars. Figure 6 displays the veiling profiles of Classical T-Tauri Stars (CTTSs), Weak-lined T-Tauri Stars (WTTSs), and non-YSOs across different wavelengths and effective temperature (T_{eff}) ranges. The veiling is shown as a function of wavelength in bins of 100K for T_{eff}. WTTSs and non-YSOs show veiling due to factors such as stellar spots.

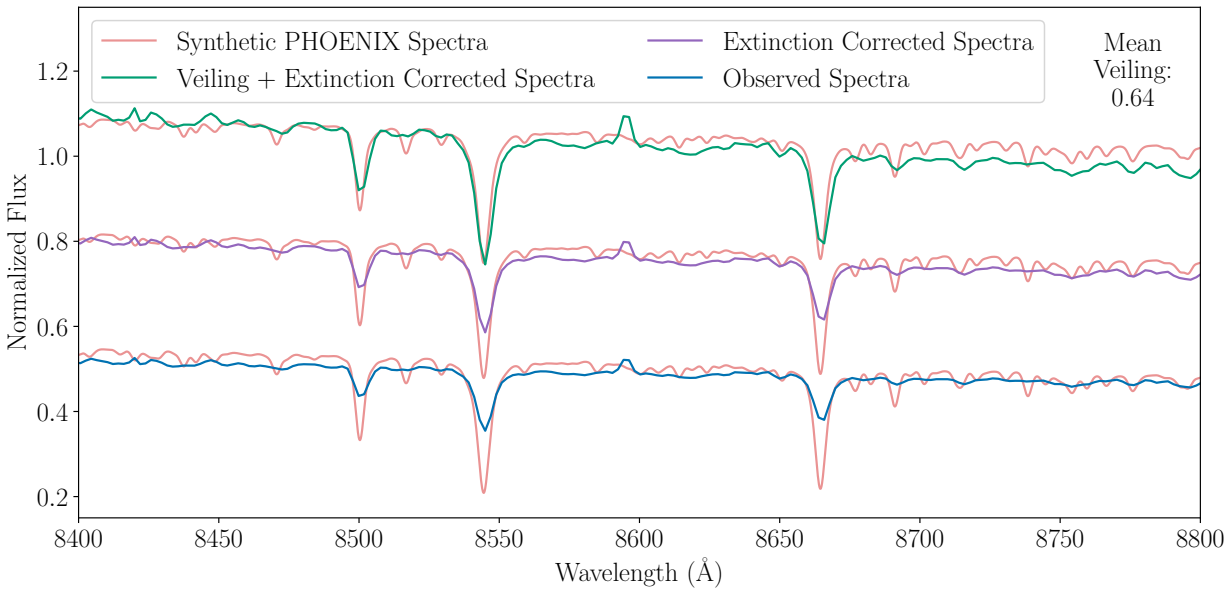

Figure 4. The observed spectra (in blue), extinction corrected spectra (in purple), and veiling + extinction corrected spectra (in green) has been plotted against the synthetic spectra model (in red). The veiling + extinction corrected spectra represent the photospheric spectra of the star. While veiling increases the photospheric flux, extinction decreases it. All the spectra are normalized and added to a constant for better visualization.

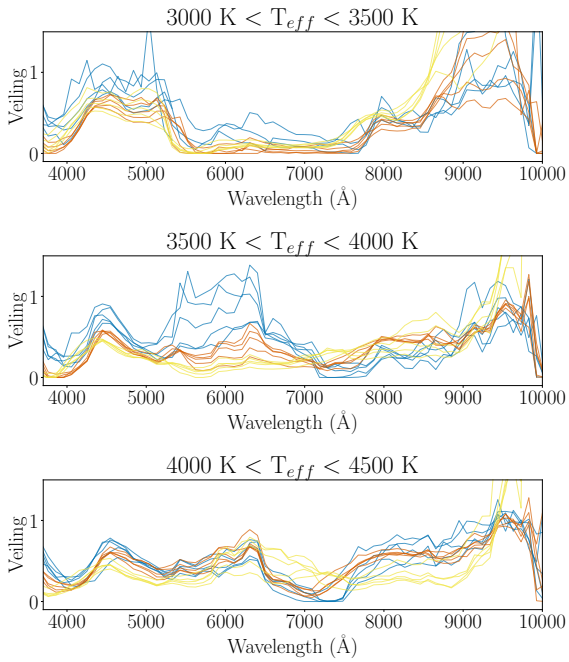

Figure 5. Veiling of CTTSs (in blue) and WTTSs (in red) and Non YSOs (in yellow) as a function of wavelength for different $T_{\rm eff}$ ranges. Each of the lines represent a bin width of 100K $T_{\rm eff}$. We see WTTSs and Non YSOSs veiling due to spots and other factors of synthetic spectra.

We also recorded the veiling uncertainty for each of the sources while calculating veiling. In all the next steps where we calculated average veiling values for further analysis, we used a weighted mean using the uncertainty in veiling as the weight. It helped us to ensure reliability against measurement variability.

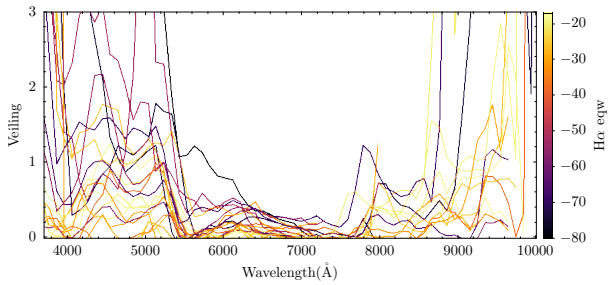

Figure 6. Corrected Veiling vs Wavelength plot for all the CTTSs in a very narrow (3330 K to 3450 K) $T_{\rm eff}$ range color coded by the Hα eqw before binning them. Each line here depicts one CTTS source. All these veiling values have been corrected by subtracting WTTSs veiling for the corresponding $T_{\rm eff}$ range.

3.3. *Correcting the veiling measurements*

The measured veiling can be affected by different systematics, some of which are wavelength dependent and some of which are dependent on the physical properties of stars like the $T_{\rm eff}$. In such cases, we corrected the initial veiling of the CTTSs.

One such case is when the spectra are affected by infrared (IR) excess. IR excess in the stellar spectra can occur due to a dusty disk around the star. This excess is

not accounted for in template matching and occurs due to a different process, which can bias veiling measurements where the IR excess is significant. For most of the sources, IR excess occurs outside of the wavelength range of the BOSS spectra. But in a handful of more extreme cases, the excess is prominent enough to be seen at the wavelength < 1 micron which is roughly the wavelength limit of BOSS spectra. To address this, the SEDFit Python package was used (Kounkel 2023). This Python module queries VizieR to download all available photometric data for a source based on its coordinates and other stellar parameters such as $T_{\rm eff}$ and $\log g$, and then performs SED fitting. The SED fitting process identifies the longest wavelength that is not affected by IR excess for each of the targeted sources by comparing the real data with a model. Thus, it is possible to determine the wavelength range from which the spectrum is affected by the IR excess. Veiling measurements were then limited to this unaffected wavelength range to ensure accuracy in the succeeding analysis.

Another important consideration are the temperature dependent systematics from the mismatch between the synthetic spectra and the real data of young stars. This is why we observed non-zero veiling in WTTSs and field stars, which do not have accretion disks and are not expected to exhibit veiling. For instance, the presence of spots in WTTSs can produce a multi-temperature spectrum that does not perfectly match the theoretical models, thereby introducing an excess veiling effect.

To correct this veiling excess, we subtracted the WTTS veiling from the CTTS veiling for each wavelength bins for all the sources. For this, we first binned the WTTSs veiling in different discrete $T_{\rm eff}$ bins starting from 2300 K to 11000 K with each bin having a size of 10 K, weighted them based on their uncertainties. Then, we subtracted the WTTSs veiling from the CTTSs veiling by matching the $T_{\rm eff}$ of CTTSs to WTTSs. This correction ensures that the veiling measurements accurately reflect the properties of the CTTSs without being influenced by systematic errors present in the theoretical models.

4. RESULTS

We expect to observe differences in the accretion properties in Classical T Tauri Stars (CTTSs) based on various factors such as effective temperature ($T_{\rm eff}$), the star's age, and the equivalent width of certain accretion sensitive lines like Hα in the spectra. The veiling and its dependence on these factors can also vary across different wavelength ranges. So we conducted a detailed investigation step for further analysis.

4.1. *Comparing with the previous studies*

There are a few previous studies that have explored the relationship between veiling and wavelength. Among these, Basri & Batalha (1990) and Ingleby et al. (2013) stand out as significant contributions because of the resolution they achieved. To compare our findings, we searched for the sources studied in these works within our sample. While no matches were found with the sources from Basri & Batalha (1990), we successfully identified two sources, CVSO 90 and CVSO 58, from Ingleby et al. (2013).

We attempted to recreate the veiling trends for these two sources as presented in Ingleby et al. (2013) and overlaid them with our data in Figure 7. Due to limited access to the original data they used, we reconstructed the plots based on visual approximations of their results. Although the curved line for CVSO 58 may not perfectly replicate the original data, it represents the best approximation achievable with our current resources. To ensure consistency, we constrained our analysis to the same wavelength ranges used in their study.

We used the following two equations to recreate the veiling trends:

For CVSO 90:

$$r_\lambda = -0.002625 \cdot \lambda + 14.675 \tag{2}$$

For CVSO 58:

$$\begin{aligned} r_\lambda = &- 0.0001575 \cdot \lambda + 1.8175 \\ &+ 5 \times 10^{-8} \cdot (\lambda - 7000)^2 - 0.2 \end{aligned} \tag{3}$$

Here in the equation, λ is wavelength in Å and r_λ is the veiling.

While comparing the veiling data from (Ingleby et al. 2013) with our own measurements, we observed notable similarities for both CVSO 90 and CVSO 58. For CVSO 90, the average veiling values align closely with those reported in the earlier study, although our data shows greater power in the UV. In the case of CVSO 58, the veiling has consistently increased across the entire wavelength range, likely due to an overall increase in accretion activity since the earlier observations were conducted. It is important to note that veiling is a highly variable quantity, driven by changes in accretion rates over time (Basri & Batalha 1990; Calvet & Gullbring 1998). Given that more than a decade has passed since the observations by (Ingleby et al. 2013), these variations are not unexpected.

4.2. *Hα Equivalent Width*

Veiling is largely produced by accretion shocks where infalling material from the circumstellar disk impacts

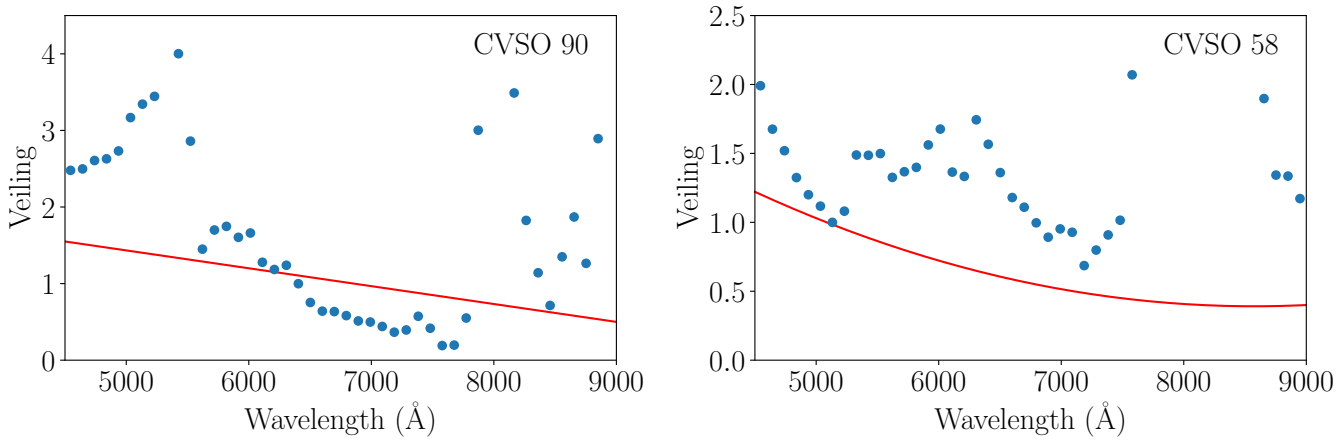

Figure 7. Matched sources from Ingleby et al. (2013). The scatter plot represents the veiling data from our study, while the red line shows a recreation of the best-fit line from Ingleby et al. (2013).

the stellar surface. This excess emission that originate from hot accretion columns and heated regions near the stellar surface can vary with temperature because the accretion process itself depends on the star's physical conditions.

The strength of Hα line in a star depends on both accretion flow and the $T_{\rm eff}$ of the system. The Hα emission produced in the accretion columns and shocks signifies intense accretion processes in the CTTSs. CTTSs with strong Hα emission will exhibit higher veiling. Also, Hα emission can be related to the $T_{\rm eff}$ of a star, so comparing the change of veiling with both Hα eqw and $T_{\rm eff}$ in different wavelength regions can be important.

To compare veiling across different temperatures, we calculated the average veiling of sources in discrete temperature bins. We separated the sources based on temperature ranges, with each bin covering a range of 100 K, considering temperatures from 3000 K to 5000 K. For each temperature bin, we calculated the average veiling array by taking the weighted mean veiling value at each wavelength across all sources within the bin, using the uncertainty in veiling as the weight. This provided a single average veiling array for each temperature range. Then to compare the veiling of CTTSs with the eqw of the Hα line, we calculated the average veiling in bins based on the eqw values. Each bin covered a range of 2 Hα eqw. We then plotted the average veiling against wavelength for each eqw bin to visualize how veiling varies with both eqw and wavelength. Finally, we made three different plots for different $T_{\rm eff}$ranges starting from 3000 K to 5000 K each of them color coded by the Hα eqw values. Figure 8 illustrates how veiling varies with both Hα eqw and wavelength across three different $T_{\rm eff}$ ranges. The veiling trends are consistent across all three temperature regions, showing three distinct peaks. The first peak occurs in the blue region, rising from the left of the plot and decreasing up to 5000 Å. The second peak is prominent in the mid-optical range, around 6000–7000 Å, where veiling reaches its maximum. Finally, there is a rise in veiling at the red end of the spectrum, beginning near 7500 Å and continuing toward 10,000 Å. When comparing veiling with Hα eqw, the relationship becomes evident: sources with Hα eqw values closer to 0 exhibit lower veiling, while sources with more negative Hα eqw values show higher veiling across all three $T_{\rm eff}$ ranges. This trend highlights the strong correlation between accretion activity, as indicated by Hα emission, and veiling.

4.3. *Ages*

Accretion flow can also vary with the age of CTTSs. As these stars age, the accretion rate from their circumstellar disks can change. Typically, as the star matures, the circumstellar disk evolves, leading to a reduction in the mass accretion rate. This decline in accretion rate results in a reduction of excess emission from accretion shocks, leading to lower veiling values in older stars. Conversely, if the accretion rate remains high or increases with age, the excess emission and veiling values can remain high or even increase.

To compare the veiling of CTTSs across different ages, we calculated the average veiling values in discrete age bins. Each age bin covered a range of 0.1 dex, and we considered ages from 1 to 30 Myr. For each age bin, we calculated the average veiling by taking the weighted mean veiling value at each wavelength for all sources within that bin, using the uncertainty in veiling as the weight. This provided a single average veiling array for each age range. We then plotted the average veiling

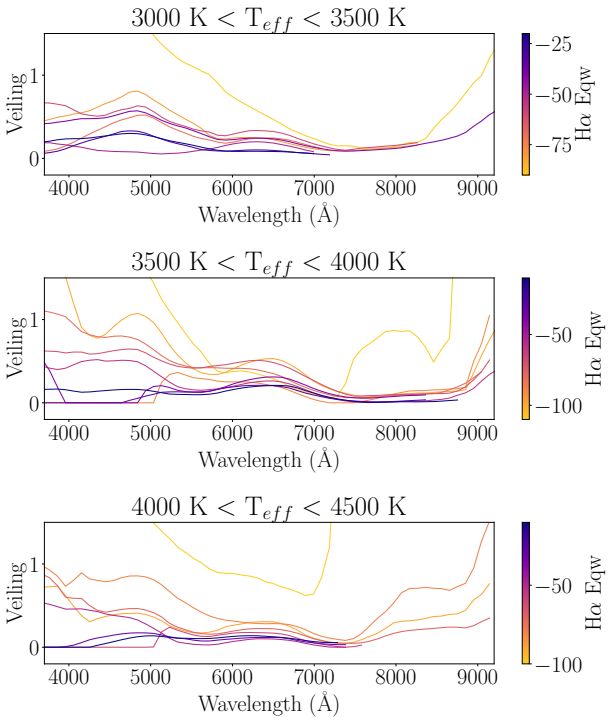

Figure 8. Corrected Veiling of CTTSs color coded by the difference between their Hα equivalent width and the CTTSs cutoff for different $T_{\rm eff}$ ranges.

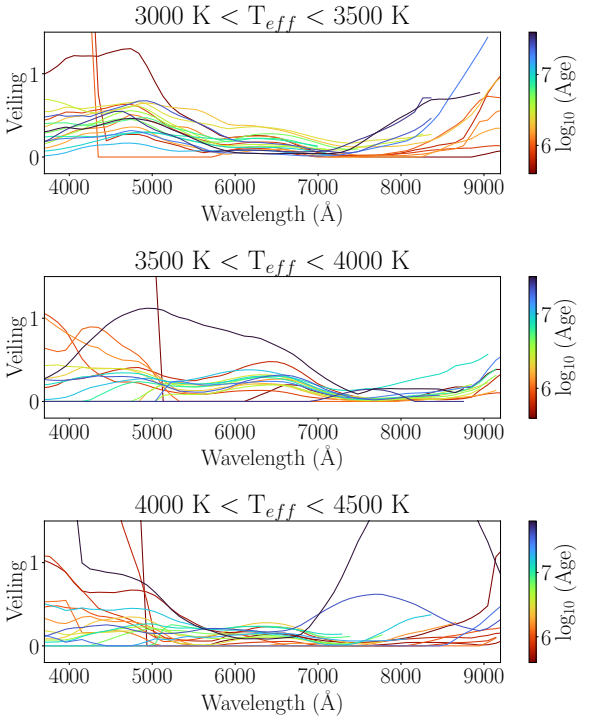

Figure 9. Corrected Veiling of CTTSs color coded by age for different $T_{\rm eff}$ ranges.

against wavelength for each age bin for four different $T_{\rm eff}$ ranges from 3000K. Figure 9 illustrates how veiling varies with both age and wavelength across four different $T_{\rm eff}$ ranges. Similar to figure 8, the veiling trends with wavelength are consistent across all temperature ranges, showing three distinct regions of veiling increase: the blue region decreasing up to 5000 Å; the mid-optical region, peaking between 6000–7000 Å; and the red region, rising beyond 7500 Å. When comparing veiling with age, however, no clear correlation emerges. The veiling values appear to vary randomly with age across the plotted temperature ranges.

5. DISCUSSION

5.1. *Wavelength Dependence*

We empirically examined the dependence of the veiling profile on wavelength. A few previous studies have done similar examination on wavelength dependence of veiling, but most of them were done for only a handful of sources (Basri & Batalha 1990; Ingleby et al. 2014; Muzerolle et al. 2003). We also found veiling not being constant throughout the wavelength ranges. In fact we found a number of features in them. First it sharply rises towards UV, starting from 3700 Å. It peaks at the blue limit of the BOSS spectra, likely increasing beyond that point. There is also a rise at the mid-optical range from 5000 Å to 7000 Å, which peaks at around 6000 Å. Finally there is a rise from 8500 Å to 10000 Å, which peaks at the red limit of the BOSS spectra. These rises of veiling at different wavelength regions can have some possible physical meanings.

The veiling rise at the UV end of the BOSS spectra from (3700 Å to 5000 Å) can be attributed to hot spots located at the accretion shock. These spots have lower filling factor as the veiling increase in this part is much lower than the veiling increase in the mid-optical region of the spectra. However, due to their high temperature (T), even a small area (A) can produce substantial luminosity (L), as described by the Stefan-Boltzmann law: $L = \sigma T^4 A$, where σ is the Stefan-Boltzmann constant (Boltzmann 1884). This relationship highlights that small, high-temperature regions can dominate the UV emission. So, these UV emitting hot spots likely have a small filling factor, which means they cover only a limited area on the stellar surface. This suggests that these regions are likely where the accretion columns directly impact the stellar surface, creating localized, high-temperature spots that contribute to the observed veiling rise without needing a large emitting area.

In the mid-optical range (5000 Å to 7000 Å), the veiling increase is more pronounced compared to the veiling rise in other regions meaning it has a higher filling factor.

But it has lower temperature contrast than the veiling increase in the UV wavelength region likely because the emitting spot in this range is cooler and closer to the stellar temperature. As luminosity (L) is proportional to surface area (A) and the fourth power of temperature (T^4), a lower temperature would require a significantly larger emitting area for the veiling effect to be noticeable. It means the veiling increase in this region is due to a more extensive surface area on the star which compensate for the lower temperature of the accretion related features. This increase can be attributed to hot spots located at the accretion shock. These spots are created by the material accreting onto the star which results in excess emission. This excess emission can change the photospheric emission more than other wavelength regions which is why it has this higher filling factor. The UV-emitting spots are possibly nested within the larger, cooler spots observed in the mid-optical range. The higher-energy spots appear to be embedded inside the broader spots of the mid-optical region.

At longer wavelengths, particularly in the 8500 Å to 10,000 Å range, the apparent increase in the veiling is likely due to not accretion, but rather due to photospheric spots on the star's surface. These spots are distinct from other surface features and contribute significantly to the veiling at these wavelengths. Although it is also true that due to low resolution spectra, there was significant noise at the longer wavelength regions which may also cause a discrepancy in the veiling values at the longer wavelength range.

5.2. *Hα Equivalent Width*

The Hα eqw is an important spectral diagnostics for understanding the accretion processes in CTTSs. As the dominant hydrogen emission line, Hα is a direct probe of the material flowing from the circumstellar disk onto the stellar surface. The strength of the Hα emission is directly related to the amount of hydrogen present in the accretion stream. Therefore, stars with stronger accretion activity tend to show larger Hα eqw values, which corresponds to higher mass accretion rates ($\dot{M}$). Numerous studies have demonstrated this relationship between Hα emission and accretion, with stronger Hα emission linked to higher accretion rates (Hartigan et al. 1994; White & Basri 2003; Manara et al. 2014; Wilson et al. 2022).

In addition to its connection to accretion, the Hα eqw provides insights into the temperature and density of the accretion flow. Higher veiling, often associated with enhanced accretion activity, also correlates with stronger Hα emission. In the Hα eqw plots (Figure 8), we observe that stars with more negative eqw values exhibit higher veiling, while stars with eqw values near to 0 show lower veiling. This trend is more clear upto a wavelength of 7000 Å and particularly in the wavelength regions where the veiling is has increased from the continuum. We also found that weaker Hα sources tend to exhibit a weaker UV excess, with their veiling concentrated predominantly in the mid-optical wavelengths. On the other hand, the stars with stronger Hα emission exhibit more pronounced veiling across the UV and optical ranges. In the $T_{\rm eff}$ region of 3500 K to 4000 K of figure 8, this trend is the most prominent. Ingleby et al. (2014) found a similar trend where they compared energy flux of accretion shock model with normalized flux. It confirms that our results are consistent with expectations that stars with stronger Hα emission, indicative of higher accretion rates, exhibit higher veiling values.

5.3. *Effective Temperature*

The effective temperature ($T_{\rm eff}$) of a star has a relation with the Hα emission. Though Hα emission is commonly used as an indicator of accretion, $T_{\rm eff}$ itself is not a direct indicator of the presence of an accretion disk.

In our study, we compared the veiling profiles across three different temperature ranges (3000 K $< T_{\rm eff} <$ 3500 K, 3500 K $< T_{\rm eff} <$ 4000 K and 4000 K $< T_{\rm eff} <$ 4500 K) in both figure 8, and figure 9). We found the change of veiling to be consistent. The veiling shows no clear dependence on $T_{\rm eff}$ as the veiling profile remains almost similar across all the three different $T_{\rm eff}$ regions.

5.4. *Age*

Veiling can also have a relationship with the age of the CTTSs. This variation can be driven by various factors that influence the accretion processes throughout a CTTSs different stages of development. In theory, as CTTSs evolve and approach the later stages of their pre-main sequence phase, we would expect a gradual decrease in accretion rates as circumstellar disks dissipate (Strom et al. 1993; Gullbring et al. 1998). As a star ages, this disk typically thins. This can lead to the star's mass loss, and the star becomes less capable of sustaining the high accretion rates observed in younger CTTSs. So, the older CTTSs should exhibit a lower veiling compared to the younger CTTSs.

The result from our analysis in figure 9 suggests that the relationship between veiling and age is more complex than a simple linear decrease. While it is true that, on average, older CTTSs tend to show lower veiling, there are notable exceptions. One such example can be the TW Hydra (Herczeg et al. 2023) which is an old star but shows signicant accretion activity. Similarly,

some younger CTTSs can also exhibit lower accretion activity. This demonstrates that the dissipation of the disk and the decrease in veiling is not strictly age dependent. Rather, the accretion activity is subject to a range of other factors. The scatter in accretion strengths across different ages is significant, even though the general trend points to a gradual decrease in accretion over time. This variability highlights that stars lose their disks in a probabilistic manner, with some stars retaining their disks and continuing to accrete for much longer periods, while others lose their disks rapidly within less than 1 Myr. Thus, while age correlates with a decrease in veiling, this trend is less pronounced than the more direct relationship between Hα emission and accretion strength.

6. CONCLUSIONS

We selected a few thousand BOSS sources to understand their accretion activity through veiling. These sources include CTTSs, WTTSs, and field stars. We calculated the extinction using and de-reddened the spectra for all the sources. Then we measured veiling for a selected number of BOSS sources in discrete wavelength ranges.

Next, we compared the veiling of CTTSs, WTTSs, and field stars. We found veiling for WTTSs and field stars due to the systematics. To correct the veiling of CTTSs for this systematics we binned the veiling of WTTSs for discrete $T_{\rm eff}$ bins and then subtracted the WTTSs veiling from CTTSs. Then we compared the corrected veiling of CTTSs with different physical properties of the CTTSs. These properties include wavelength, Hα eqw, $T_{\rm eff}$, and age of the stars.

We found veiling having different features across different wavelengths. Some of these features are attributed to the behavior of the accretion stream and spots on the accretion disk while some of these features are not related to the accretion activity of the stars.

We also found veiling to be related to both Hα eqw and $T_{\rm eff}$. More Hα eqw means more veiling. On the other hand, some of the features in veiling were found to be prominent for some $T_{\rm eff}$ regions. We also found that the peak of the veiling in mid-optical region is moving towards redder wavelengths for lower eqw values.

Finally, we compared veiling with age where we found that veiling can differ for stars throughout its ages. Sometimes some old stars can still remain active and show high veiling and some stars can show low veiling even if they are young.

Software: TOPCAT (Taylor 2005), BOSS Net (Sizemore 2024) , AstroPy (Astropy Collaboration et al. 2022), LineForest (Kounkel et al. 2023), Sagitta (McBride et al. 2021)

ACKNOWLEDGMENTS

This work has made use of data from the European Space Agency (ESA) mission *Gaia* (https://www.cosmos.esa.int/gaia), processed by the *Gaia* Data Processing and Analysis Consortium (DPAC, https://www.cosmos.esa.int/web/gaia/dpac/consortium). Funding for the DPAC has been provided by national institutions, in particular the institutions participating in the *Gaia* Multilateral Agreement.

REFERENCES

Alcalá, J. M., Manara, C. F., Natta, A., et al. 2017, A&A, 600, A20, doi: 10.1051/0004-6361/201629929

Astropy Collaboration, Price-Whelan, A. M., Lim, P. L., et al. 2022, ApJ, 935, 167, doi: 10.3847/1538-4357/ac7c74

Basri, G., & Batalha, C. 1990, ApJ, 363, 654, doi: 10.1086/169374

Bertout, C. 1989, ARA&A, 27, 351, doi: 10.1146/annurev.aa.27.090189.002031

Bessolaz, N., Zanni, C., Ferreira, J., Keppens, R., & Bouvier, J. 2008, A&A, 478, 155, doi: 10.1051/0004-6361:20078328

Boltzmann, L. 1884, Annalen der Physik, 258, 291, doi: 10.1002/andp.18842580616

Calvet, N., & Gullbring, E. 1998, ApJ, 509, 802, doi: 10.1086/306527

Espaillat, C. C., Herczeg, G. J., Thanathibodee, T., et al. 2022, AJ, 163, 114, doi: 10.3847/1538-3881/ac479d

Fischer, W. J., Hillenbrand, L. A., Herczeg, G. J., et al. 2023, in Astronomical Society of the Pacific Conference Series, Vol. 534, Protostars and Planets VII, ed. S. Inutsuka, Y. Aikawa, T. Muto, K. Tomida, & M. Tamura, 355, doi: 10.48550/arXiv.2203.11257

Gahm, G. F., Walter, F. M., Stempels, H. C., Petrov, P. P., & Herczeg, G. J. 2008, A&A, 482, L35, doi: 10.1051/0004-6361:200809488

Gordon, K. 2024, The Journal of Open Source Software, 9, 7023, doi: 10.21105/joss.07023

Gullbring, E., Hartmann, L., Briceño, C., & Calvet, N. 1998, ApJ, 492, 323, doi: 10.1086/305032

Hartigan, P., Edwards, S., & Ghandour, L. 1994, in American Astronomical Society Meeting Abstracts, Vol. 185, American Astronomical Society Meeting Abstracts, 48.15

Hartmann, L., Herczeg, G., & Calvet, N. 2016, ARA&A, 54, 135, doi: 10.1146/annurev-astro-081915-023347

Herczeg, G. J., Chen, Y., Donati, J.-F., et al. 2023, ApJ, 956, 102, doi: 10.3847/1538-4357/acf468

Husser, T.-O., Wende-von Berg, S., Dreizler, S., et al. 2013, A&A, 553, A6, doi: 10.1051/0004-6361/201219058

Ingleby, L., Calvet, N., Hernández, J., et al. 2014, ApJ, 790, 47, doi: 10.1088/0004-637X/790/1/47

Ingleby, L., Calvet, N., Herczeg, G., et al. 2013, ApJ, 767, 112, doi: 10.1088/0004-637X/767/2/112

Kounkel, M. 2023, mkounkel/SEDFit: 0.3, 0.3, Zenodo, doi: 10.5281/zenodo.8076501

Kounkel, M., Zari, E., Covey, K., et al. 2023, ApJS, 266, 10, doi: 10.3847/1538-4365/acc106

Kounkel, M., Saad, S., Lane, K., et al. 2023, LineForest, 1.0, Zenodo, doi: 10.5281/zenodo.10279307

Manara, C. F., Testi, L., Natta, A., et al. 2014, A&A, 568, A18, doi: 10.1051/0004-6361/201323318

McBride, A., Lingg, R., Kounkel, M., Covey, K., & Hutchinson, B. 2021, AJ, 162, 282, doi: 10.3847/1538-3881/ac2432

Morbidelli, A., & Raymond, S. N. 2016, Journal of Geophysical Research (Planets), 121, 1962, doi: 10.1002/2016JE005088

Muzerolle, J., Hillenbrand, L., Calvet, N., Briceño, C., & Hartmann, L. 2003, ApJ, 592, 266, doi: 10.1086/375704

Pittman, C. V., Espaillat, C. C., Robinson, C. E., et al. 2022, AJ, 164, 201, doi: 10.3847/1538-3881/ac898d

Robinson, C. E., & Espaillat, C. C. 2019, ApJ, 874, 129, doi: 10.3847/1538-4357/ab0d8d

Romanova, M. M., Ustyugova, G. V., Koldoba, A. V., & Lovelace, R. V. E. 2002, ApJ, 578, 420, doi: 10.1086/342464

Saad, S., Lane, K., Kounkel, M., et al. 2024, AJ, 167, 125, doi: 10.3847/1538-3881/ad2001

Shu, F., Najita, J., Ostriker, E., et al. 1994, ApJ, 429, 781, doi: 10.1086/174363

Sizemore, L. 2024, hutchresearch/BOSSNet: BOSS Net v1.0.0, 1.0.0, Zenodo, doi: 10.5281/zenodo.10453135

Sizemore, L., Llanes, D., Kounkel, M., et al. 2024, arXiv preprint, doi: 10.48550/arXiv.2402.05184

Smee, S. A., Gunn, J. E., Uomoto, A., et al. 2013, AJ, 146, 32, doi: 10.1088/0004-6256/146/2/32

Stock, C., McGinnis, P., Caratti o Garatti, A., Natta, A., & Ray, T. P. 2022, A&A, 668, A94, doi: 10.1051/0004-6361/202244315

Strom, S. E., Edwards, S., & Skrutskie, M. F. 1993, in Protostars and Planets III, ed. E. H. Levy & J. I. Lunine, 837

Taylor, M. B. 2005, in Astronomical Society of the Pacific Conference Series, Vol. 347, Astronomical Data Analysis Software and Systems XIV, ed. P. Shopbell, M. Britton, & R. Ebert, 29

White, R. J., & Basri, G. 2003, ApJ, 582, 1109, doi: 10.1086/344673

Wilson, T. J. G., Matt, S., Harries, T. J., & Herczeg, G. J. 2022, MNRAS, 514, 2162, doi: 10.1093/mnras/stac1397